Title

An Easy to Manufacture Micro Gas Preconcentrator for Chemical Sensing Applications

Journal

ACS Sensors, 2(8)

ISSN

2379-3694

Authors

McCartney, Mitchell M

Zrodnikov, Yuriy

Fung, Alexander G

et al.

Publication Date

2017-08-25

DOI

10.1021/acssensors.7b00289

Peer reviewed

HHS Public Access

Author manuscript

ACS Sens. Author manuscript; available in PMC 2019 May 29.

Published in final edited form as:

ACS Sens. 2017 August 25; 2(8): 1167–1174. doi:10.1021/acssensors.7b00289.

AN EASY TO MANUFACTURE MICRO GAS PRECONCENTRATOR FOR CHEMICAL SENSING APPLICATIONS

Mitchell M. McCartney[1], **Yuriy Zrodnikov**[1], **Alexander G. Fung**[1], **Michael K. LeVasseur**[1], **Josephine M. Pedersen**[1], **Konstantin O. Zamuruyev**[1], **Alexander A. Aksenov**[1], **Nicholas J. Kenyon**[2,3], and **Cristina E. Davis**[*,1]

[1]Mechanical and Aerospace Engineering, University of California Davis, Davis, CA 95616

[2]Department of Internal Medicine, Division of Pulmonary and Critical Care Medicine, University of California, Davis, Sacramento, CA 95617

[3]Center for Comparative Respiratory Biology and Medicine, University of California, Davis, Davis, CA 95616

Abstract

We have developed a simple-to-manufacture microfabricated gas preconcentrator for MEMS-based chemical sensing applications. Cavities and microfluidic channels were created using a wet etch process with hydrofluoric acid, portions of which can be performed outside of a cleanroom, instead of the more common deep reactive ion etch process. The integrated heater and resistance temperature detectors (RTDs) were created with a photolithography-free technique enabled by laser etching. With only 28 V DC (0.1 A), a maximum heating rate of 17.6 °C/s was observed. Adsorption and desorption flow parameters were optimized to be 90 SCCM and 25 SCCM, respectively, for a multi-component gas mixture. Under testing conditions using Tenax® TA sorbent, the device was capable of measuring analytes down to 22 ppb with only a 2 min sample loading time using a gas chromatograph with a flame ionization detector. Two separate devices were compared by measuring the same chemical mixture; both devices yielded similar peak areas and widths (FWHM: 0.032-0.033 min), suggesting reproducibility between devices.

Graphical Abstract

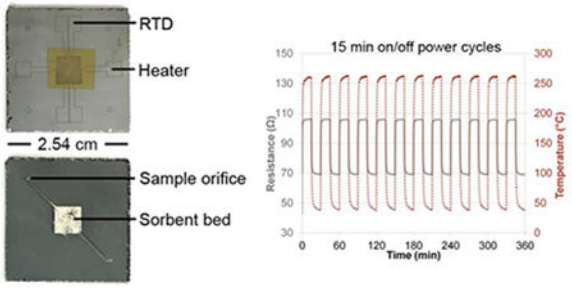

[*]Corresponding author: cedavis@ucdavis.edu.

CONFLICT OF INTEREST DISCLOSURE

The authors declare that a patent application has been submitted on part of the work presented in this paper.

Keywords

gas preconcentrator; micro electromechanical systems (MEMS); chemical sensor; sorbent; detectors

Miniaturization of devices and systems has been a pronounced trend over the past decade. Of particular interest is the development of microelectromechanical systems (MEMS)-based chemical sensors and associated component technologies. In many applications, the sensor must meet minimum criteria (low cost, portability, reliability, robustness). Often, detection of certain compounds can be particularly challenging in the presence of interfering background matrices. Furthermore, sensitivity and selectivity toward the target compound are especially critical to minimize false negatives. To enhance detection, many sensing platforms perform a preconcentration of the chemical sample. Preconcentration can both increase the limit of detection and improve selectivity by reducing matrix interferences and/or rejecting undesirable compounds. Thus, MEMS-based gas sensors can benefit from a micro gas preconcentrator (μPC)[1]. This has been demonstrated in systems such as micro gas chromatographs[2–6] and organic vapor sensors.[7–10]

Generally, μPCs prioritize miniaturization and low power consumption over high sorbent capacity.[11–12] Still, certain key variables affect preconcentration and cannot be compromised. Devices should achieve high adsorption flows, low desorption flows and increased limits of detection.[7,13] Precise thermal management is also of particular importance.[14–15]

Both the design of the preconcentrator and sorbent can be tailored to specific applications. A significant amount of preconcentrator development is dedicated to environmental monitoring, such as benzene detection,[16–17] or for atmospheric pollution.[18–20] Typically, μPCs contain a sorptive region, such as a microcavity that is either filled or coated with a sorbent. For example, the commercially available sorbent Tenax®, poly(2,6-diphenyl-p-phenylene oxide), has a weak affinity for water, making it a useful sorbent to preconcentrate volatiles from human breath or other high-humidity matrices. Sorbents either adsorb or absorb analytes depending on their chemical properties. Gaseous samples can be introduced either by actively flowing through the sorptive region via an air pump or through passive exposure to the analytic environment. After sampling, the device is rapidly heated and the analytes are released from the sorbent (desorption). A carrier gas directs the preconcentrated vapors to the downstream detection system.

While many researchers continue to develop novel μPCs for specific applications, other groups may only require a basic gas preconcentrator for developing new chemical sensors or systems-level devices. In the present work, we have designed and manufactured a robust micro gas preconcentrator using relatively straight forward MEMS processes. The device is amenable to many chemical sensing applications as it can easily be packed or printed with commercially available sorbents and provides flexibility, low cost and ease of manufacturing. Herein we describe the simple manufacturing process and present data that showcase the device’s optimal performance, such as robust thermal management and manufacturing reproducibility. Furthermore, we experimentally determine appropriate

adsorption and desorption flow rates. Data were generated by coupling our micro gas preconcentrator to a gas chromatograph system (GC) with a flame ionization detector (FID) for proof-of-concept demonstration.

EXPERIMENTAL SECTION

μPC MANUFACTURING PROCESS

A visual of the micro gas preconcentrator is provided (Figure 1). The front side of the device contains the integrated heater and RTD elements. The heater runs across the central sorbent cavity. RTD 1 runs within the center of the sorbent cavity and RTD 2 runs along the outside of the sorbent cavity. These two RTDs allow users to monitor any possible temperature differences that exist between the middle of the sorbent cavity and the edges.

Parts of this fabrication process were performed in a class-100 cleanroom facility (Center for Nano and Micro Manufacturing, UC Davis, CA). A summary of the process is provided (Figure 2).

The μPC manufacturing processes use thoroughly cleaned (4:1 Piranha solution for 20 min), rinsed and dried (N_2 stream) borosilicate glass wafers (Borofloat® 33 by Schott Co.), 100 mm in diameter and 0.7 mm thick, as working media. This type of glass, due to its chemical composition and fabrication method, is heat amenable and can withstand multiple rapid heating and cooling cycles, having a direct benefit to our work. No quantitative comparison was done with other types of borosilicate glasses but the material is chosen per manufacturer's specifications. The fabricated chips demonstrated excellent practical reliability in multiple operational cycles (data follows).

A reliable masking layer is required to etch the deep cavity for the sorbent material. Photoresists have poor adhesion with a glass surface and cannot create a reliable masking for wet etching of glass in hydrofluoric acid; therefore, a bilayer chromium-photoresist mask was prepared.[21] A chromium layer enhances photoresist adhesion to the surface but is prone to pin-hole defects that act as precursors for the mask damage in wet etch. A spin-coated photoresist layer covers defects in the metal layer. Thus, a combination of chromium and photoresist layers creates a reliable mask for wet etching of glass in HF acid solution.

A 200 ± 28 nm thick chromium layer was deposited with an electron beam evaporator (CHA Industries AutoTech II, Fremont, CA) on the front side of the wafers. The pattern of the microchannel and cavity was defined with lithography of positive tone photoresist, SPR™ 220-7.0 (Dow® Electronic Materials MEGAPOSIT™, Malborough, MA). The wafers were spin-coated with hexamethyldisilazane (HMDS) reagent at 2 kRPM followed by spin-coating of the photoresist also at 2 kRPM. The prepared mask was soft-baked at 95 °C for 5 min and UV exposed to 250 mJ/cm^2 for 15 sec (Karl Suss, MA4, hard contact, broadband UV wave-lengths of 365, 405 and 436 nm, Garching, Germany). The photoresist was developed in aqueous developer, Microposit MF CD-26 (Dow Electronic Materials, Malborough, MA) with gentle manual agitation for 2 min. The mask was hard-baked in a vacuum oven at 155 °C for 90 min and allowed to cool slowly. The back side of the wafer was covered with a layer of Parafilm® tape (Bemis, Sheboygan Falls, WI) to prevent glass

etching from the back side of the wafer. The prepared wafer was dipped into chromium etchant (Transene Chromium Etchant 1020, Danvers, MA) to define the pattern of the microchannel and sorbent cavity in the chromium layer of the mask. When the pattern was visually transparent, the wafer was removed from the etchant bath, cleaned with DI water and dried with N2. The sorbent cavity and microchannel were created by etching in 49% HF acid bath for 1.25 h with no agitation, resulting in an etch depth of approximately 350 μm.

The wafer was diced into individual dies, each 2.54 × 2.54 cm^2, with a dicing saw (Disco DAD 321, Japan). The inlet and outlet sample orifices were drilled into half of the glass chips using a diamond-plated drill having ~0.8 mm diameter. To create a complete chip, each of the drilled dies were paired with one of the non-drilled dies and bonded together in a glass-to-glass thermal fusion bonding procedure (a steady pressure of approximately 20 kPa is applied on two glass parts in contact through two parallel stainless steel plates at 580 °C for 4 h). Fiducial markers were used to ensure that microfluidic channels and the sorbent cavity were aligned. A single 100 mm diameter borosilicate wafer yielded seven glass dies, enough for three chips and one spare die. To ensure bonded chips were airtight, a pressure of 3.4 atm of helium was applied at one sample orifice using our custom flow and electronic fixture (described in the following **Flow & Electronics Fixture** section). A commercial He detector (Part 22655, Restek, Bellafonte, PA) was used to ensure the chip did not leak.

The chip-integrated heating element was fabricated on the non-drilled side of the μPC. The surface opposite of the side with drilled holes was sputtered with a layer of Chromium–Tungsten–Chromium having thicknesses of 20–1000–20 nm. The sputtering rate was ~13 nm/min with a total time of 75 min. Sputtering was performed in an argon environment at a pressure of 5 mTorr with 300 W of power. A heating element pattern was defined with a commercial diode-pumped solid-state laser (Samurai UV Marking/Micromachining System, model 3530-30; wavelength 355 nm UV, equipped with a telecentric lens, F=103 mm; DPSS Lasers, Santa Clara, CA). The laser parameters were set to 40 passes at 1.5 Watt, 70 kHz frequency, and 100 mm/s scan speed. The side with the laser-patterned heating element was thoroughly cleaned with dry nitrogen flow to remove all laser generated particles of conductive material that could short-circuit the electrical pattern of the heating element. Then, a 400 nm layer of SiO2 was deposited on the central heater area of the heating element to reduce oxidation at high temperatures. The contact pads were covered with a shadow mask during the SiO_2 deposition in the electron beam evaporator.

In our present work, the μPCs were packed with Tenax® TA sorbent (Sigma-Aldrich, St. Louis, MO). A glass wool plug was introduced to one orifice and a vacuum was applied. Tenax® was introduced on the opposite orifice and was pulled by the vacuum through the sorbent bed, filling it. Once the sorbent bed was packed, another glass wool plug was inserted to prevent the granular sorbent from being expelled by gas flow from the cavity.

A heat transfer simulation of the device was performed using COMSOL Multiphysics (COMSOL Inc.). The chip was modeled as a 3D object with the actual geometry and material of the final device (1.4 mm thick borosilicate glass). There were six structural contacts with the chip, which were neglected from the model for simplicity: two low-thermally conductive PTFE O-rings on one side and two pogo pins and two more PTFE O-

rings on the opposite side. This assumption was based on the substantial distance from the active heating area for these connection points and the low thermal conductivity of borosilicate glass to allow significant heat to conduct to these points. The boundary conditions consisted of a free convective layer of air at 293 K around the top and bottom surfaces (convective heat transfer coefficient, h, of 10 W/m*K), a forced convective layer of helium at 293 K through the microchannels and sorbent cavity (h=30 W/m*K), and radiation-to-ambient-air from the top and bottom surfaces (surface emissivity, ε, of 0.79 for silica). Power was directly applied to the surface of the active area through the heater geometry. The model used Newton's Law of Cooling for convective heat transfer and the Stefan-Boltzmann Law for radiative heat transfer. In these equations, q is the heat transferred per unit time, A is surface area, σ is the Stefan-Boltzmann constant, T_h is the temperature of the hotter medium or surface and T_c is the temperature of the colder medium or surface.

$$q = hA(T_h - T_c) \quad (1)$$

$$q = \varepsilon\sigma(T_h^4 - T_c^4)A \quad (2)$$

The energy (E) per analysis cycle of our preconcentrator was determined from the length of time (t) that power (P) is applied to the heater, using the set voltage (V) and the resulting current (I). From Joule's Law and the definition of power:

$$P = V \cdot I \quad (3)$$

$$E = P \cdot t = V \cdot I \cdot t \quad (4)$$

FLOW & ELECTRONICS FIXTURE

For chemical adsorption and desorption, the μPC was placed in a custom built fixture consisting of a top and bottom housing. The bottom housing contained a custom PCB with pogo pins to establish the electrical contacts for RTD measurements and heater voltage. To reduce the amount of heat that could dissipate from the device, thermal contact to the bottom of the housing was limited to only the pogo pins and two PTFE O-rings. The top housing had two compression fitting adapters with a 1/16" male NPT end. This end had also been machined out slightly to enable the PTFE O-ring to sit inside and extend outward from the fitting. The two PTFE O-rings were the only point of contact with the μPC from the top of the housing. The two parts of the fixture were connected through four 6-32 screws that adjusted how tightly the housings fit together.

The electronics of the setup were controlled using an Arduino Uno R3 microcontroller that communicated to a computer via a serial port. RTD measurements were sampled by an

ADS1248 (Texas Instruments, Dallas, TX) 24-bit analog to digital converter (ADC) configured in a 4-wire RTD sampling setup. These measurements were recorded every 0.5 sec. Timing of events was performed through the internal clock on the Arduino Uno. The heaters were switched on and off through a MOSFET. For RTD calibration, temperature measurements were performed by attaching a thermocouple to the outside of the sorbent cavity, held in place by thermal paste. Temperature measurements were recorded every 1 sec using a multimeter.

µPC ADSORPTION/DESORPTION

A commercially available 25 component gas mixture (Part 34434, Restek, Bellafonte, PA) was used to generate calibration curves and to optimize adsorption and desorption flow rates. The mixture contained a range of compounds with disparate chemical and physical properties that represent common environmental contaminants. All compounds were present at 1 ppm in grade 5 ultra-pure nitrogen. The mixture was diluted with helium using two mass flow controllers (Figure 3). During adsorption, the ambient temperature of the µPC was maintained at 40 °C and the components were sampled for 2 min. Resulting GC-FID data from five adsorption flow rates (30, 60, 90, 120, 150 and 180 SCCM) and three desorption flow rates (5, 15, 25 SCCM) were compared. Flow rates of 90 and 25 SCCM for adsorption and desorption, respectively, were used to generate the calibration curve. Each concentration was measured 5 times in randomized sample order. For desorption, 28 V were applied across the µPC heater for 15 min, which reached a final temperature of 260 °C.

An 8-port valve connected the µPC to the other test rig components, such as to the sample mixture and also to the GC-FID. For adsorption, a vacuum was applied to one end of the device and the diluted sample mixture was introduced at the opposite end using two MFCs (Figure 3). For desorption, helium carried the analytes to the inlet of the GC-FID by fused silica transfer lines that were maintained at 200 °C and connected with Valco® compression fittings. The fused silica was inserted as far into the GC inlet as possible, which had a 0.75 mm straight inlet liner (Part 23434, Restek, Bellefonte, PA) installed to minimize dead volume.

For µPC device comparison and preconcentration factor calculations, the headspace of a mixture containing 3-carene, D-limonene and 1-nonanal in ethanol was used (Sigma-Aldrich, St. Louis, MO), using the apparatus just described. To calculate the preconcentration factor,[7] we compared an empty µPC with no sorbent to the same device packed with sorbent. Both received the same adsorption/desorption treatments.

GC-FID SETTINGS

For chemical detection, we employed an HP 5890 gas chromatograph with flame ionization detector (GC-FID, Agilent Technologies, Santa Clara, CA). Separation occurred on a DB-VRX capillary column (20 m × 0.18 mm × 1.00 µm, Agilent Technologies, Santa Clara, CA). The injection port was set to 235 °C, splitless injection. The GC oven was initially set to 35 °C and held for 5 min while the volatiles in the µPC desorbed. Then the oven was ramped to 170 °C at 10 °C/min, then to 250 °C at 30 °C/min and held for 3.33 min. The FID

was set to 250 °C. Numerical analysis for peak detection and integration was performed with Agilent's Enhanced ChemStation (F.01.00.1903, Santa Clara, CA).

RESULTS AND DISCUSSION

In the present work, we describe our micro gas preconcentrator. A visual of the device is provided (Figure 1). Its manufacturing process avoids traditional deep reactive ion etch (DRIE) and instead involves a wet etch process for flow channels. The following data demonstrate that the chip is robust and amendable to many micro chemical sensing applications.

MANUFACTURING PROCESS

Typically, micro gas preconcentrators are fabricated using a deep reactive ion etch (DRIE) process to create the sorbent cavity and flow channels.[3, 7, 12,18, 22–23] This technique requires specialized machines in a cleanroom facility. We created our cavities through a wet etch process using an acid bath (HF, Figure 2), which can be performed outside of clean room facilities. There was no problem with particles during the fabrication and bonding processes because the size of the etched cavity and the microchannels are sufficiently large. Manual liquid washing and blowing with compressed nitrogen were sufficient for cleaning, thus negating the need of a cleanroom for this step. Furthermore, our group has recently developed a photolithography-free method to etch microfluidic structures in university settings.[21] Other manufacturing steps, such as glass cleaning, drilling, laser patterning of the heater elements and bonding steps can be potentially done without the use of a clean room facility but done in a wet-sink equipped laboratory. Deposition of metal film for masking layer can be outsourced if one purchases metallized glass wafers from a vendor. Thus the entire fabrication process is easy and has the potential for cost-savings. This benefits users who may be focused on developing new chemical sensors and need an amendable, easy to manufacture micro gas preconcentrator for their work.

Passivation layers are common industrial practices and our work agrees with this sentiment. The silicon dioxide layer was integral, as μPCs without this coating displayed evidence of oxidation within the heater wires and RTDs. Two common afflictions due to oxidation were that the initial RTD resistance increased at ambient temperature after each heating cycle, making temperature calibration impossible, and that the heaters lost functionality. Devices lasted less than a dozen heating cycles. RTV silicone, gold and aluminum oxide were tested but failed to prevent oxidation of the heater/RTD wires below. Insulation of the Chromium–Tungsten–Chromium heating element with the SiO_2 layer established its repeatable performance over many cycles, vastly increasing the durability of our chips as they survived over 100 cycles.

During heater/RTD manufacturing development, a total of 18 μPCs with the same cavity and microchannel dimensions were packed with Tenax® and held 6.994 ± 0.821 mg of sorbent.

TEMPERATURE/RTD DATA

The heat transfer of the device was modeled. We provide a visualization of the model (Figure 4) when equilibrium is reached between heating and convective/radiative cooling.

The simulation predicted a required input power of approximately 2.5 W for the full active area, or sorbent bed, to reach a minimum of 260 °C, with more localized heating occurring at the heater surface.

A comparison of an externally applied thermocouple and RTD1 resistance was conducted (Figure 5). A 30 min heating/cooling cycle (28 V DC applied across heater, ~0.1 A, for 15 min, then no voltage for 15 min) was conducted twelve consecutive times. The inceptive (ambient) temperature was 40 °C. After heating, a temperature of 260 °C was measured with a thermocouple at the center of the sorbent cavity (opposite face of the heater/RTD components).

The heating rate affects how quickly volatiles desorb. Slower heating rates will increase the amount of time VOCs release from the sorbent. This will cause a stream, rather than burst, of compounds to enter the gas chromatography system, broadening peaks and degrading data quality. Faster heating rates lead to sharper chromatographic peaks and thus higher limits of detection.[7] For our device, the temperature increased rapidly and consistently, heating from 40 °C to 200 °C in 30 sec (average heating ramp of first 30 sec, 5.40 ± 0.03 °C/sec). With only 28 V DC applied to the heater, a maximum increase of 17.6 °C/s was observed. Other researchers have reported maximum desorption heating rates of 2.67 °C/s,[7, 19] 10.0 °C/s,[12] 13.4 °C/s[24] and 25 °C/s.[18] Compared to these devices, our preconcentrator heats at a relatively fast rate. The faster heater rate previously reported[18] is likely due to that device only having a ~200 nm coating of Tenax® within their sorbent cavity whereas our devices were packed with ~7 mg of Tenax® grains. This mass difference may contribute to our slower heating ramp. Faster desorption rates in our device can likely be achieved by decreasing the sorbent cavity, which would reduce the mass to be heated but would decrease detection limits due to the reduced amount of sorbent, or by increasing the heater voltage, which would increase power consumption. Both the RTD resistance and the thermocouple measurements remained stable after the device reached its desorption temperature. Even without an active cooling element, the μPC cooled to its ambient temperature in approximately 2 min. This allowed for adsorption onto the μPC to simultaneously occur while the GC oven cooled to its initial temperature value (35 °C), reducing downtime between samples, making this device amendable to high throughput applications.

Using Equation 4, the energy per analysis cycle was calculated. With a voltage of 28 V DC at 0.1 A of current, the energy used to heat the device from 40 °C to 200 °C in 30 sec was 84 J. For one extended cycle, where the device was heated and held at 260 °C for a total time of 15 min, the energy per cycle was 2.5 kJ.

FLOW OPTIMIZATION

Adsorption and desorption flow influences device performance and should be optimized for sample matrices, as these parameters can have varying effects on different analytes (data follows). An equation for sample concentration (C), flow rate (f) and sample time (t) during adsorption (a) and desorption (d) from mass conservation provides:

$$C_a \cdot f_a \cdot t_a = C_d \cdot f_d \cdot t_d \quad (5)$$

Hence, the ratio of desorption concentration and adsorption concentration is given by:

$$\frac{C_d}{C_a} = \frac{f_a \cdot t_a}{f_d \cdot t_d} \quad (6)$$

So, higher adsorption flow rates and lower desorption flow rates theoretically yield better chemical detection.[7]

We optimized both flow conditions for our sample mixture. Twelve compounds were compared by measuring the GC-FID peak areas that resulted from six different adsorption flows (Figure 6). For this experiment, desorption was set to 25 SCCM. We observed that detector responses increased as adsorption flow increased for some compounds (4-ethyltoluene, benzyl chloride, 2-hexanone, dibromochloromethane, 2-methyl-2-pentanone). Other compounds were observed to have decreased response with higher adsorption flow (vinyl bromide, allyl chloride, methyl tert-butyl ether, 1.3-butadiene). An adsorption flow of 90 SCCM was chosen as it yielded acceptable peak areas with minimum sample volume. A similar experiment was performed with three desorption flows (5, 15 and 25 SCCM, data not shown) using an adsorption flow of 90 SCCM. Conversely, lower desorption flows typically produced better detection.[7] Many compounds could not be detected with a desorption flow of 5 SCCM. For desorption, 25 SCCM resulted in the best peak shape and detector response. Under these conditions, three compounds (4-ethyltoluene, benzyl chloride and 2-hexanone) were detected as low as 22 ppb. Using other more sensitive detection methods, this LOD might be even lower.

Per Equation 6, longer adsorption times could increase detection capabilities lower than 22 ppb. In the present study, we limited sample time to 2 min to conserve the sample mixture. Other variables (GC inlet and FID temperatures, e.g.) were not optimized for this study and could further improve results. We note that optimal parameters depend on sample matrices and encourage users to perform such experiments for their compounds of interest.

CHEMICAL DETECTION

A comparison of an empty μPC (no sorbent) and the same device packed with Tenax® revealed that our device did indeed preconcentrate chemical samples and improve chemical detection. To quantify this enhancement, preconcentration factors are typically reported. This factor is a ratio of the detector response of the preconcentrated sample to a non-preconcentrated sample (an indication of signal improvement due to preconcentration). A comparison of 3-carene, D-limonene and 1-nonanal revealed preconcentration factors of 5.1, 13.7 and 10.3 respectively.

Under our analytical conditions (2 min sample time, 90 SCCM adsorption, 25 SCCM desorption, Tenax® TA sorbent), we were able to detect 4-ethyltoluene, benzyl chloride and 2-hexanone down to 22 ppb (Figure 7). Detection limits could be increased by further optimization, especially sampling time.[7] We built a calibration curve of four concentrations (22, 100, 256 and 667 ppb), collecting $n=5$ measurements per concentration. Each compound yielded a linear detector response with increased concentration (R^2 values: 4-

ethyltoluene 0.989, benzyl chloride: 0.982, 2-hexanone 0.989). The linearity indicates that sorbent did not reach saturation under sampling conditions and thus further sensitivity gains may be possible.

Other micro gas preconcentrators systems using Tenax® report similar detection capabilities. One previously reported device with precipitated Tenax® columns reported 1 ppb detection of alkanes but did not disclose sample time in their manuscript. Thus, their time could be significantly higher than our 2 min.[25] Another Tenax®-packed device reported limits of 25 ppb.[18] A third device using precipitated columns and a micromechanical sensing system detected as low as 160 ppb.[26] Thus, we confirm that our device operates within acceptable concentration levels.

DEVICE REPLICATES

Two separately manufactured micro gas preconcentrators were compared (Figure 8). Both devices yielded nearly identical detector responses (peak areas) when measuring three chemicals (3-carene, D-limonene and nonanal, Table 1). No statistical differences between the peak areas of two devices were observed using a student's t-test ($p<0.05$). Peak widths were nearly identical between the two devices, suggesting that the desorption heating rate was sufficiently similar between the devices. A slight retention time shift existed but was found to be minimal (approximately 0.028 min, easily corrected by data processing).

The resistance across the RTDs and heater shows variability between devices. Heater, RTD 1 and RTD 2 resistances on one device were 249.5, 89.6 and 60.1 Ω respectively while on another device were 277.3, 100.8 and 64.9 Ω. This is likely due to small manufacturing differences during the deposition of the Cr-W-Cr layer and/or during the laser-cutting process. Per the peak area and FWHM results (Table 1), the resistance difference did not affect data quality (both devices had 28 V applied across the heater during desorption). However, the differences in RTD resistance mean that each device would need to be calibrated independently should temperature information be required.

CONCLUSIONS

We have developed a micro gas preconcentrator to enhance MEMS-based chemical sensing platforms. By etching microfluidic channels with a wet etch process, we have reduced the cost and time to manufacture our device. We optimized device parameters and detected several compounds down to 22 ppb. A comparison of two devices shows that the manufacturing process is reproducible. Furthermore, the devices are durable, lasting over 100 heating/cooling cycles in this current experimental setup.

We believe that this device will provide MEMS researchers with an easy to manufacture micro gas preconcentrator so that their focus can remain on chemical sensing development. The device has a simple design and can be packed or printed with many commercially available sorbents (and is thus suitable for a variety of sample matrices) and making it amendable to a potentially wide range of applications.

ACKNOWLEDGMENTS

Partial support was provided by: the Hartwell Foundation (CED), the NIH National Center for Advancing Translational Sciences (NCATS) through grant #UL1 TR000002 (CED, NJK); NIH award U01 EB0220003-01 (CED, NJK); NIH award 1P30ES023513-01A1 (CED, NJK); NIH award UG3-OD023365 (CED, NJK) and NSF award #1255915 (CED, AAA). Student support was provided by NIH award T32 HL07013 (KOZ), NIH award #P42ES004699 (KOZ), and a National Science Foundation Graduate Research Fellowship Program (JMP). The contents of this manuscript are solely the responsibility of the authors and do not necessarily represent the official views of the funding agencies.

REFERENCES

1. Voiculescu I; Zaghloul M; Narasimhan N, Microfabricated chemical preconcentrators for gas-phase microanalytical detection systems. TrAC Trends in Analytical Chemistry 2008, 27 (4), 327–343.
2. Lu CJ; Steinecker WH; Tian WC; Oborny MC; Nichols JM; Agah M; Potkay JA; Chan HKL; Driscoll J; Sacks RD; Wise KD; Pang SW; Zellers ET, First-generation hybrid MEMS gas chromatograph. Lab Chip 2005, 5 (10), 1123–1131. [PubMed: 16175269]
3. James F; Breuil P; Pijolat C; Camara M; Briand D; Bart A; Cozic R, Development of a MEMS Preconcentrator for Micro-gas Chromatography Analyses. Procedia Engineering 2014, 87, 500–503.
4. Terry SC; Jerman JH; Angell JB, A gas chromatographic air analyzer fabricated on a silicon wafer. IEEE Transactions on Electron Devices 1979, 26 (12), 1880–1886.
5. Zarejan-Jahromi MA; Ashraf-Khorassani M; Taylor LT; Agah M, Design, Modeling, and Fabrication of MEMS-Based Multicapillary Gas Chromatographic Columns. J Microelectromech S 2009, 18 (1), 28–37.
6. Lewis PR; Manginell P; Adkins DR; Kottenstette RJ; Wheeler DR; Sokolowski SS; Trudell DE; Byrnes JE; Okandan M; Bauer JM; Manley RG; Frye-Mason C, Recent advancements in the gas-phase MicroChemLab. IEEE Sensors Journal 2006, 6 (3), 784–795.
7. Camara M; Breuil P; Briand D; Viricelle JP; Pijolat C; de Rooij NF, Preconcentration Modeling for the Optimization of a Micro Gas Preconcentrator Applied to Environmental Monitoring. Anal Chem 2015, 87 (8), 4455–4463. [PubMed: 25810264]
8. Dua V; Surwade SP; Ammu S; Agnihotra SR; Jain S; Roberts KE; Park S; Ruoff RS; Manohar SK, All-Organic Vapor Sensor Using Inkjet-Printed Reduced Graphene Oxide. Angewandte Chemie International Edition 2010, 49 (12), 2154–2157. [PubMed: 20187049]
9. Barnard SM; Walt DR, A Fiber Optic Organic Vapor Sensor. Abstr Pap Am Chem S 1990, 199, 111-Anyl.
10. Beeby SEG; Kraft M; White Neil, MEMS Mechanical Sensors. Artech House, Inc.: Norwood, MA, 2004.
11. Cook KA; Sastry AM, Influence of scaling effects on designing for power efficiency of a micropreconcentrator. J Vac Sci Technol B 2005, 23 (2), 599–611.
12. Tian WC; Wu TH; Lu CJ; Chen WR; Sheen HJ, A novel micropreconcentrator employing a laminar flow patterned heater for micro gas chromatography. J Micromech Microeng 2012, 22 (6), 1–8.
13. Manginell RP; Radhakrishnan S; Shariati M; Robinson AL; Ellison JA; Simonson RJ, Two-dimensional modeling and simulation of mass transport in microfabricated preconcentrators. Ieee Sensors Journal 2007, 7 (7–8), 1032–1041.
14. Furstenberg R; Kendziora CA; Stepnowski SV; Mott DR; McGill RA, Infrared micro-thermography of an actively heated preconcetrator device. P Soc Photo-Opt Ins 2008, 6939, U1–U12.
15. Yeom J; Field CR; Bae B; Masel RI; Shannon MA, The design, fabrication and characterization of a silicon microheater for an integrated MEMS gas preconcentrator. J Micromech Microeng 2008, 18 (12), 1–12.
16. Lahlou H; Vilanova X; Correig X, Gas phase micro-preconcentrators for benzene monitoring: A review. Sensor Actuat B-Chem 2013, 176, 198–210.
17. Lin YS; Kuo CY; Tian WC; Wu TH; Sheen HJ; Kuo HY; Lu CJ In Batch fabrication of micro preconcentrator with thin film microheater using Tollen's reaction, 2013 Transducers &

Eurosensors XXVII: The 17th International Conference on Solid-State Sensors, Actuators and Microsystems (TRANSDUCERS & EUROSENSORS XXVII), 16–20 June 2013; 2013; pp 2025–2028.

18. Garga A; Akbar M; Vejerano E; Narayanan S; Nazhandali L; Marr LC; Agah M, Zebra GC: A mini gas chromatography system for trace-level determination of hazardous air pollutants. Sensor Actuat B-Chem 2015, 212, 145–154.
19. Camara EHM; Breuil P; Briand D; Guillot L; Pijolat C; de Rooij NF, Micro gas preconcentrator in porous silicon filled with a carbon absorbent. Sensor Actuat B-Chem 2010, 148 (2), 610–619.
20. Xu BY; Wang ZY, A Microcalorimeter with a Carbon Nanotube Forest as a Preconcentrator for Trace Chemical Detection. 2015 Transducers - 2015 18th International Conference on Solid-State Sensors, Actuators and Microsystems (Transducers) 2015, 1460–1463.
21. Zamuruyev KO; Zrodnikov Y; Davis CE, Photolithography-free laser-patterned HF acid-resistant chromium-polyimide mask for rapid fabrication of microfluidic systems in glass. J Micromech Microeng 2017, 27 (1), 1–10.
22. Akbar M; Shakeel H; Agah M, GC-on-chip: integrated column and photoionization detector. Lab Chip 2015, 15 (7), 1748–1758. [PubMed: 25673367]
23. Rydosz A, Micropreconcentrators In Silicon-Glass Technology for the Detection of Diabetes Biomarkers. Inform Midem 2014, 44 (2), 126–136.
24. Dow ABA; Sklorz A; Lang W, A microfluidic preconcentrator for enhanced monitoring of ethylene gas. Sensor Actuat a-Phys 2011, 167 (2), 226–230.
25. Alfeeli B; Agah M, Toward Handheld Diagnostics of Cancer Biomarkers in Breath: Micro Preconcentration of Trace Levels of Volatiles in Human Breath. Ieee Sensors Journal 2011, 11 (11), 2756–2762.
26. Chae MS; Kim J; Yoo YK; Kang JY; Lee JH; Hwang KS, A Micro-Preconcentrator Combined Olfactory Sensing System with a Micromechanical Cantilever Sensor for Detecting 2,4-Dinitrotoluene Gas Vapor. Sensors-Basel 2015, 15 (8), 18167–18177. [PubMed: 26213944]

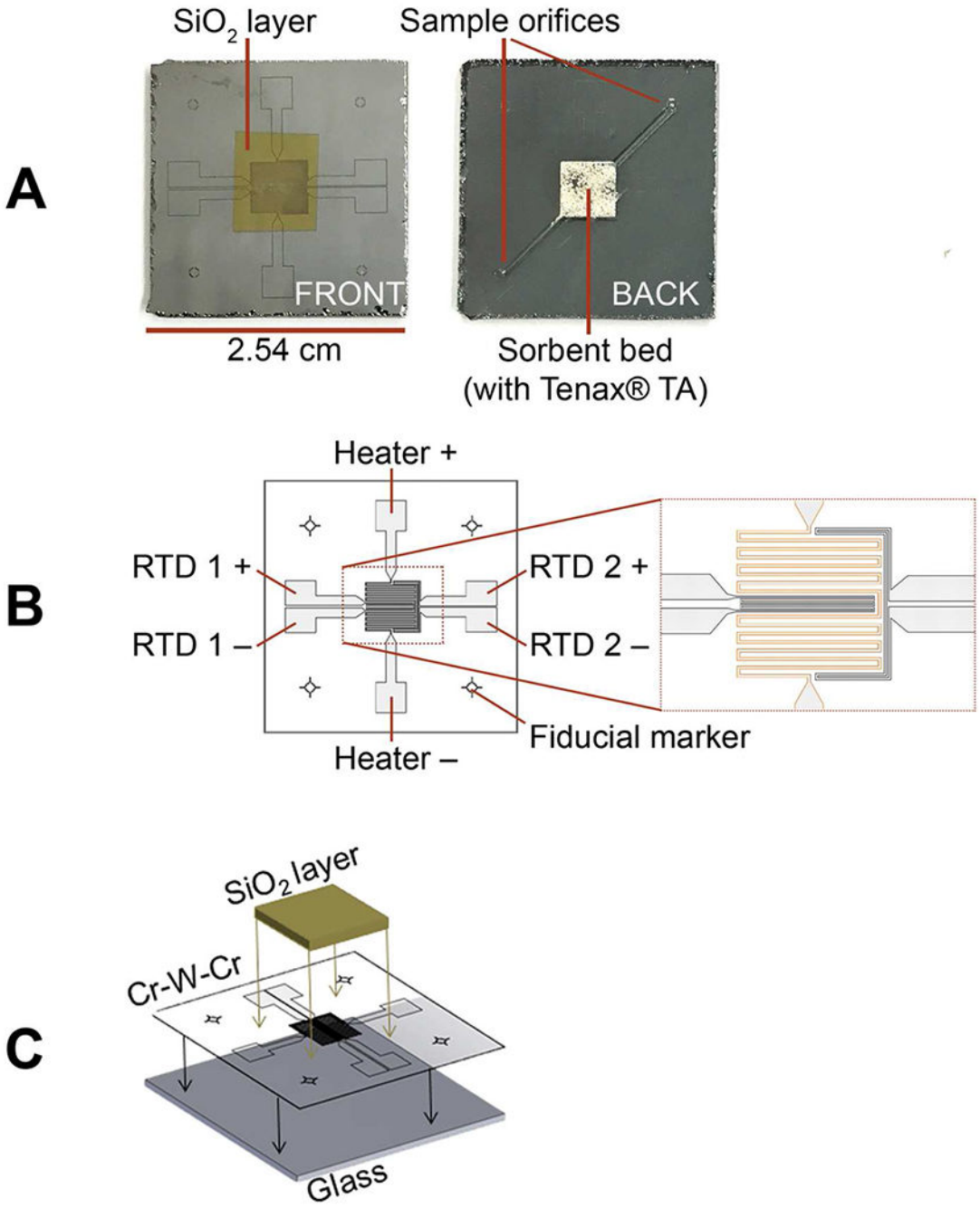

Fig 1.

The micro gas preconcentrator μPC). A) Images of both faces of the μPC B) Heater and RTD details C) Three-dimensional view of layers108×139mm (300 × 300 DPI)

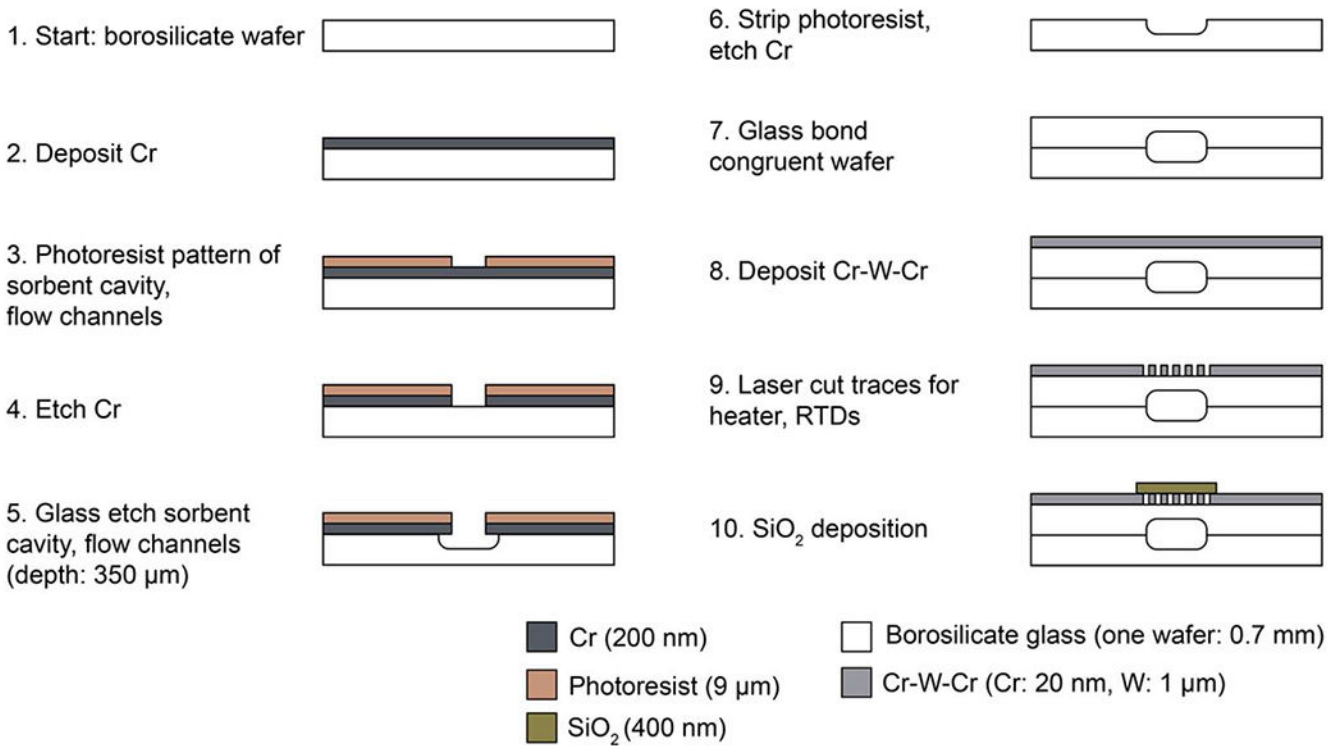

Fig 2.

μPC manufacturing process. The depth of each layer is provided in the legend 99×55mm (300 × 300 DPI)

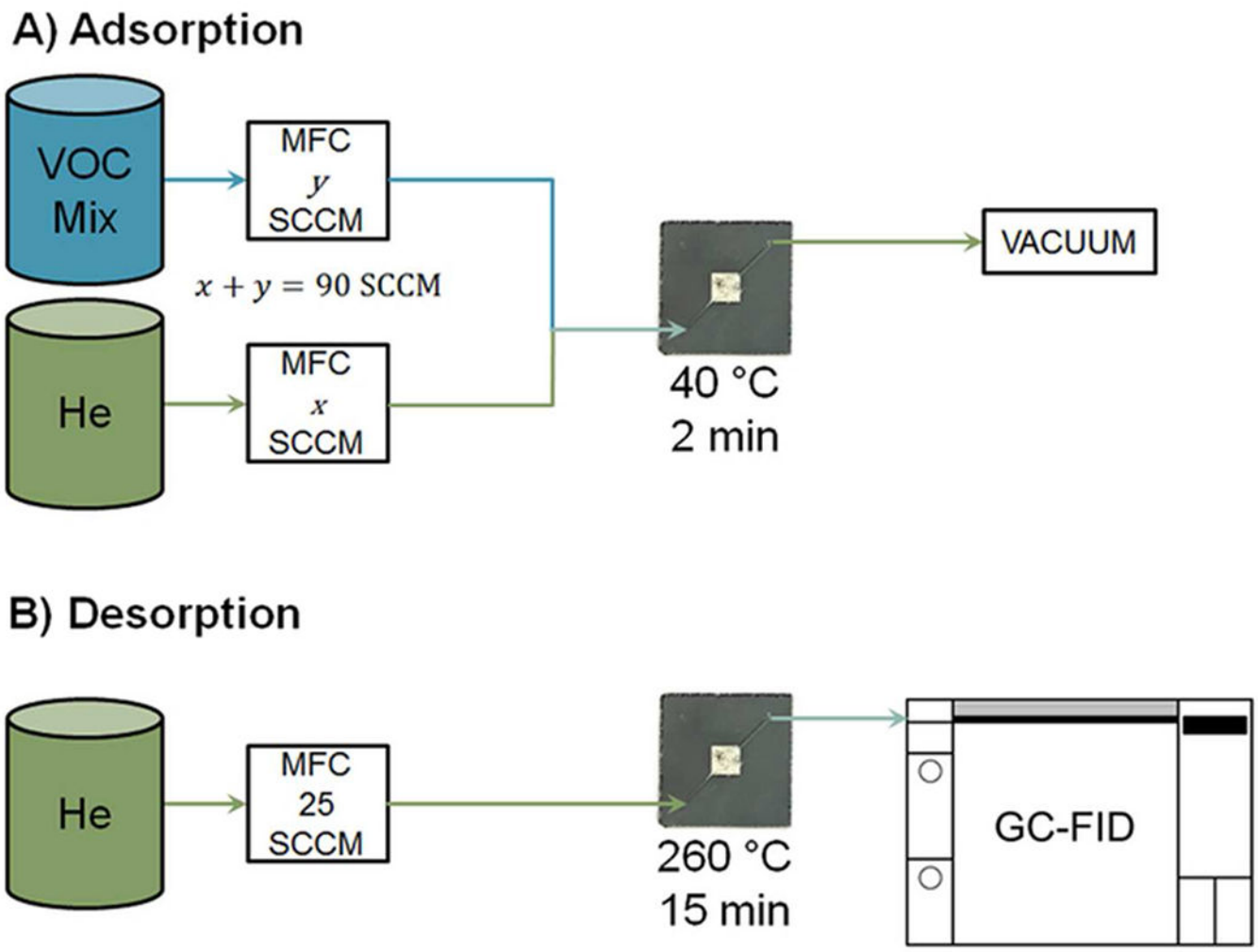

Fig 3.

Schematic of sample loading (adsorption) and GC-FID chemical analysis (desorption). A) The sample (VOC mix) was diluted with helium (He) using two mass flow controllers (MFC) for a total flow of 90 SCCM through the μPC B) Analytes are carried to the GC-FID using a flow of helium at 25 SCCM 60×43mm (300 × 300 DPI)

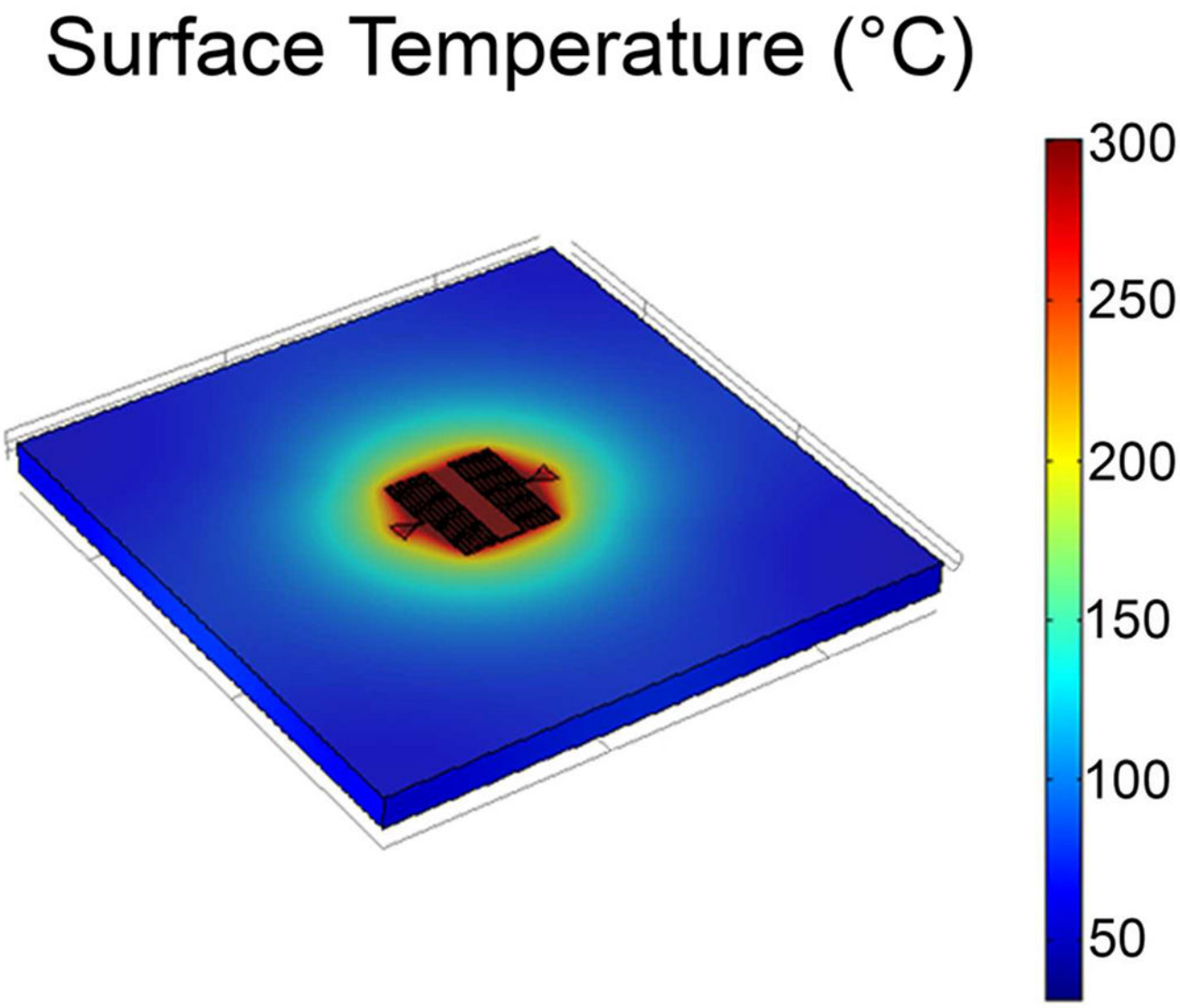

Fig 4.

Model of heat transfer. The power required to achieve a temperature of 260 °C at the sorbent cavity was calculated to be 2.5 W 70×59mm (300 × 300 DPI)

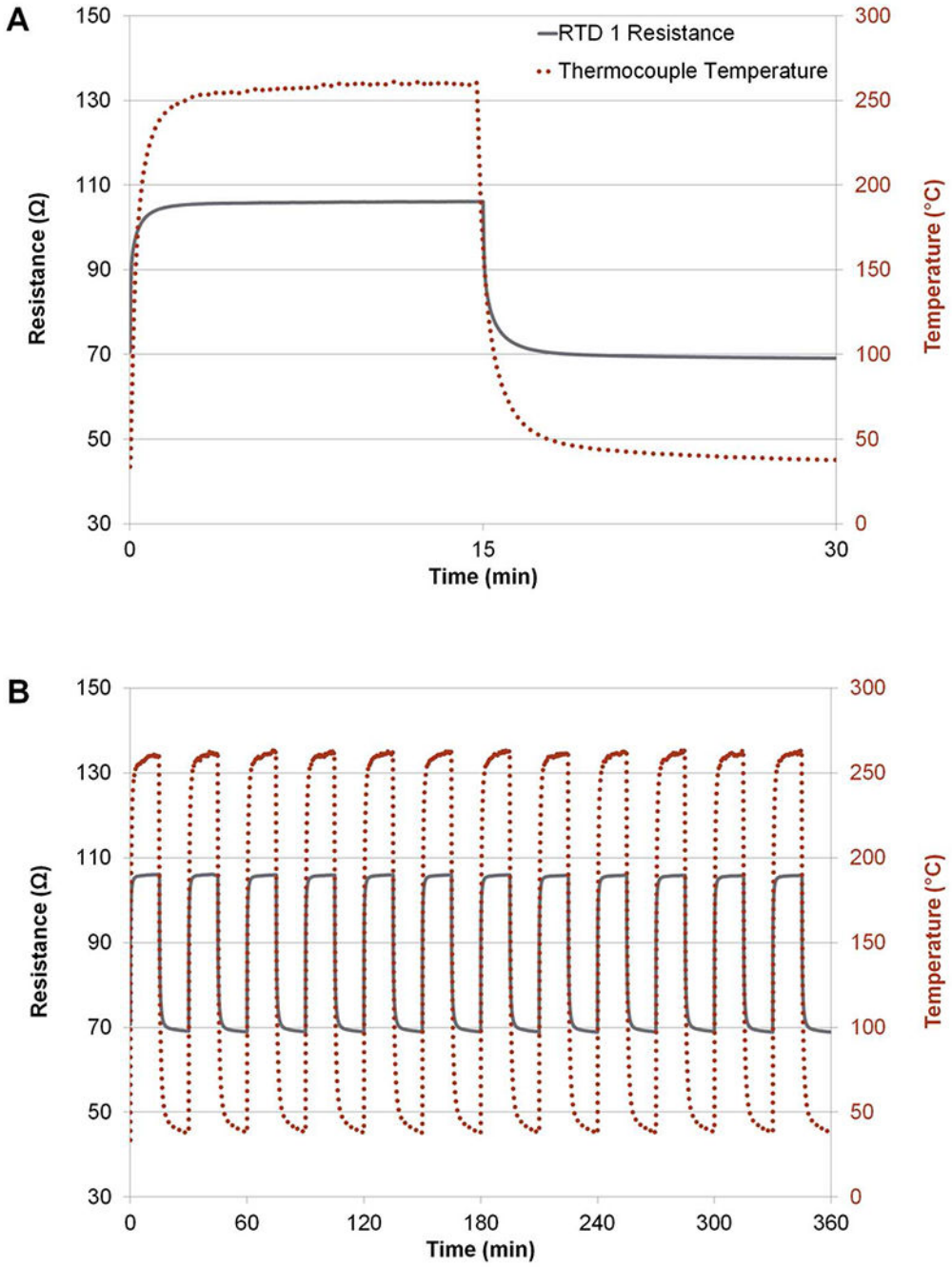

Fig 5.

Comparison of RTD 1 resistance measurements from the μPC and temperature measurements from an externally applied thermocouple. Each cycle consisted of 28 V applied across the heater for 15 min (heating) followed by no voltage for 15 min (cooling). A) Close up of one cycle B) Twelve consecutive cycles. A maximum heating rate of 17.6 °C/s was observed 106×132mm (300 × 300 DPI)

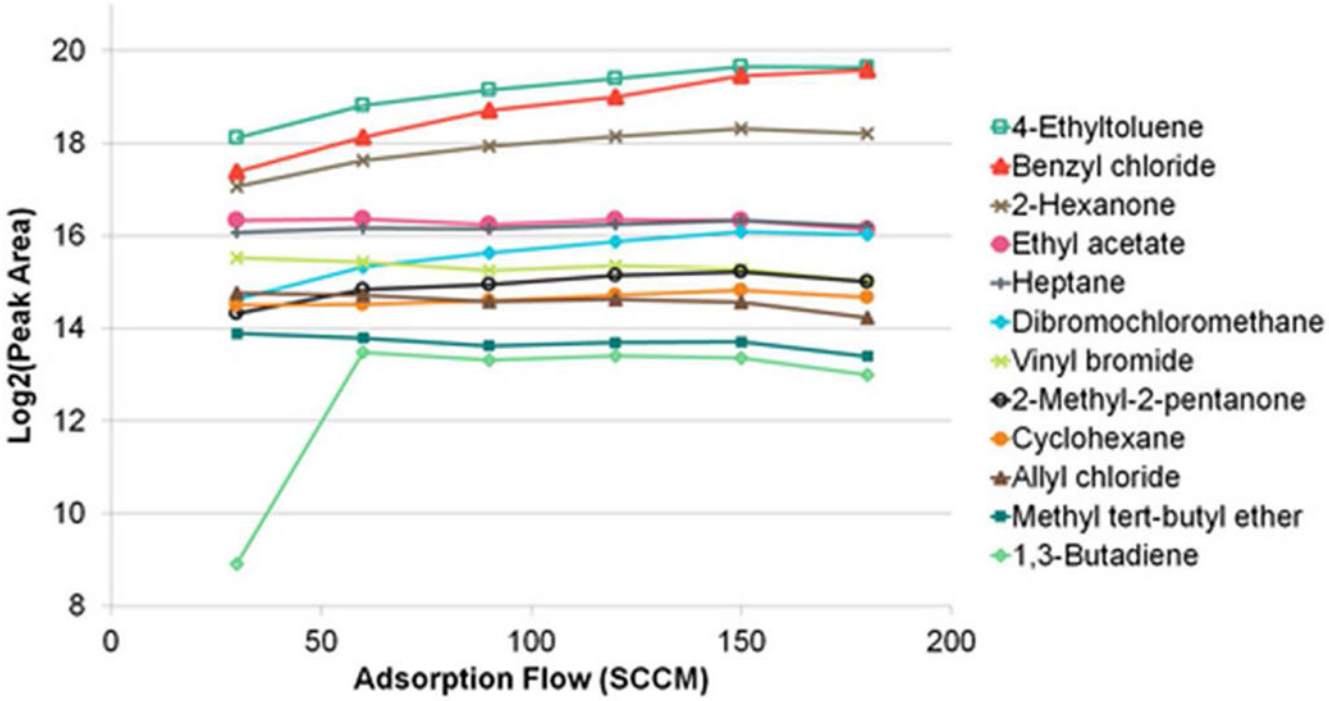

Fig 6.

Effect of sample adsorption flow through the μPC on detector response (GC-FID data). Each point is the average of n=2 samples. Ultimately, an adsorption flow of 90 SCCM was chosen for this sample matrix (acceptable peak areas with minimal sample volume) 45×24mm (300 × 300 DPI)

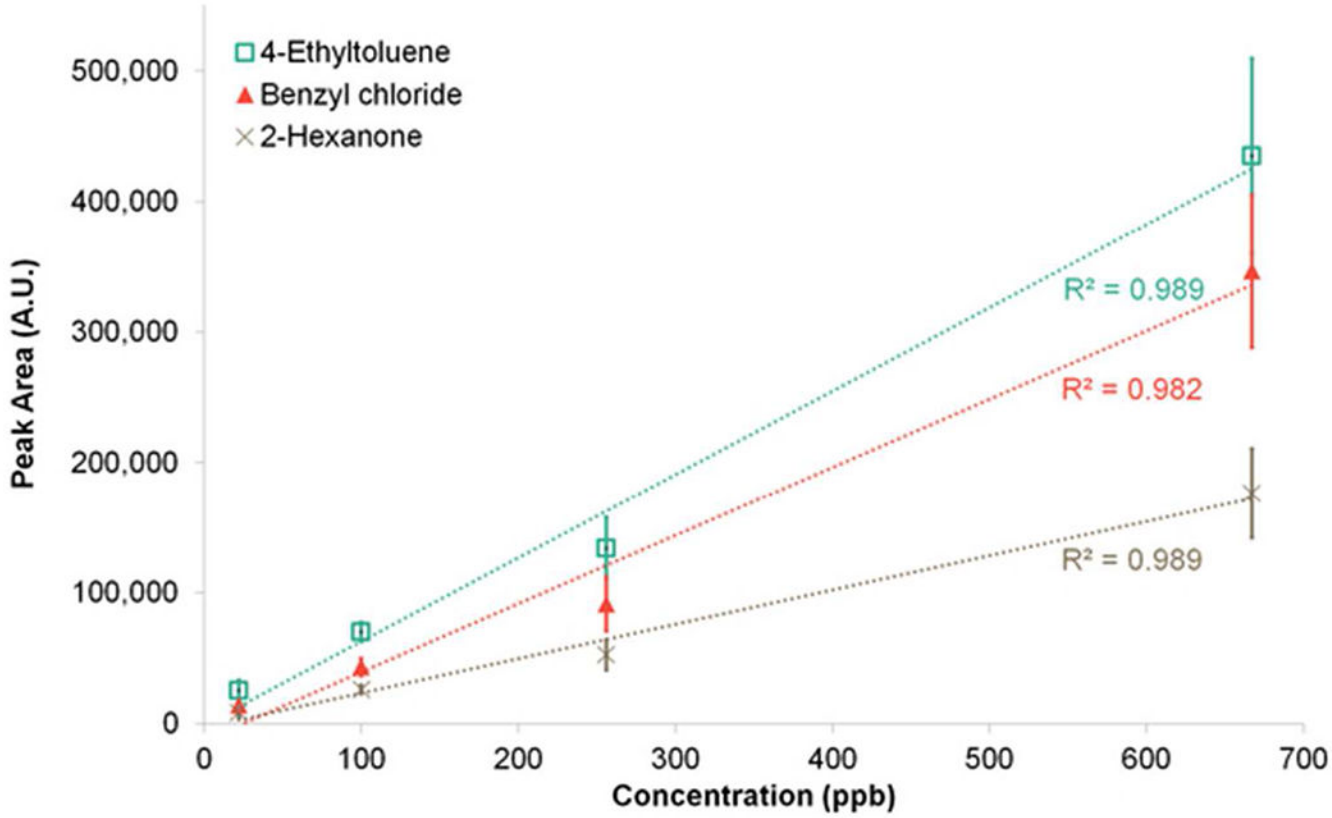

Fig 7.

Calibration curve of 4-ethyltoluene, benzyl chloride and 2-hexanone measured with the μPC-GC-FID. Each point is the average of n=5 measurements; one standard deviation is shown 50×30mm (300 × 300 DPI)

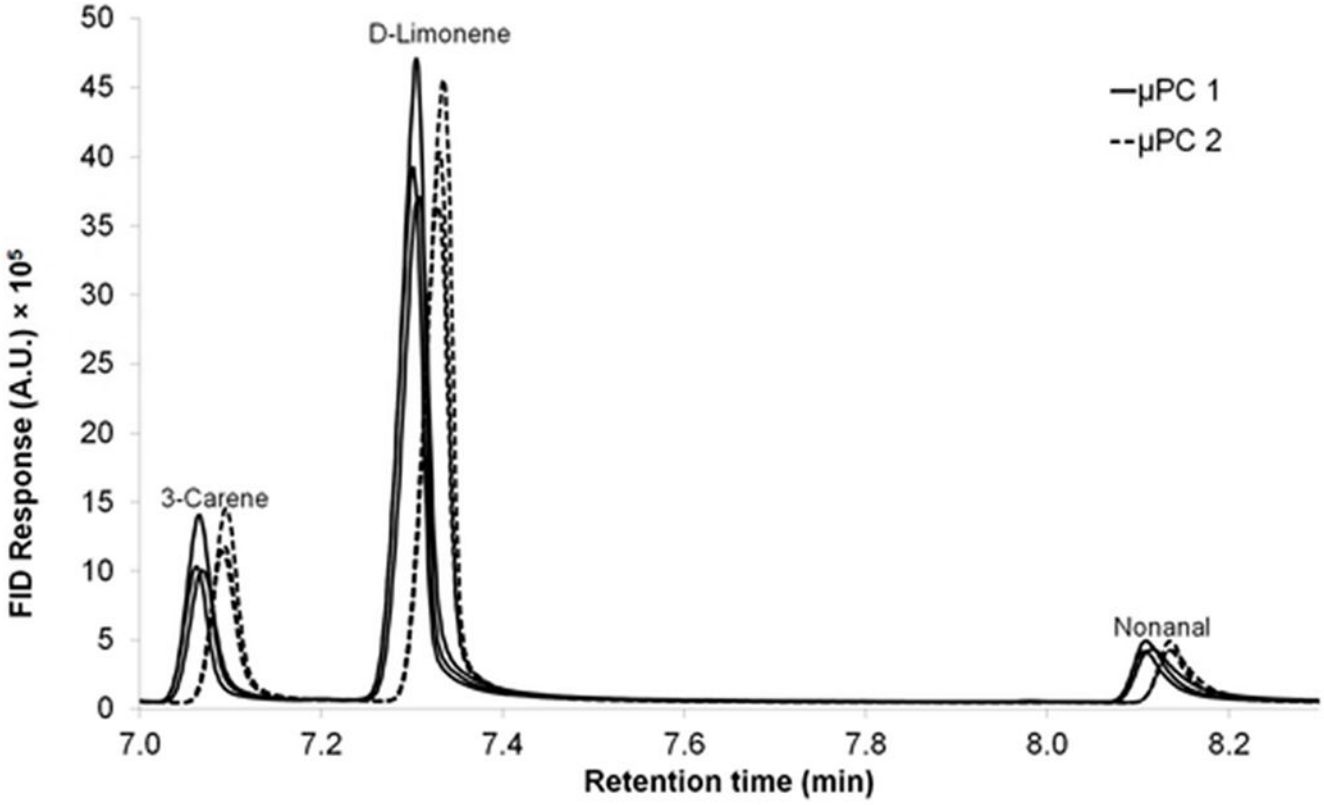

Fig 8.

GC-FID response of two µPCs (n = 3 per µPC). A slight retention time shift existed between the two devices (approx. 0.028 min) but both yielded similar data quality, measured by peak area and peak width, of the three compounds 48×27mm (300 × 300 DPI)

TABLE 1:

Detector responses for three VOCs as measured using two different micro gas preconcentrators. Shown are peak are averages of n=3 samples with standard deviations shown (in arbitrary units). Retention times (RT) and peak full widths at half maximum (FWHM) are shown in minutes.

	3-Carene		
	Peak Area	**RT**	**FWHM**
μPC 1	2,440,194 ± 443,140	7.064 ± 0.002	0.032 ± 0.001
μPC 2	2,551,034 ± 332,580	7.092 ± 0.002	0.032 ± 0.001
	D-Limonene		
	Peak Area	**RT**	**FWHM**
μPC 1	9,452,474 ± 940,743	7.303 ± 0.002	0.033 ± 0.001
μPC 2	8,798,377 ± 949,643	7.330 ± 0.003	0.033 ± 0.001
	Nonanal		
	Peak Area	**RT**	**FWHM**
μPC 1	1,456,510 ± 355,511	8.108 ± 0.002	0.046 ± 0.002
μPC 2	1,202,900 ± 111,224	8.136 ± 0.002	0.043 ± 0.005